Received: 4 July 2019 | Revised: 28 February 2020 | Accepted: 5 March 2020

DOI: 10.1111/ffe.13223

Check for updates

ORIGINAL CONTRIBUTION

FFEMS Fatigue & Fracture of Engineering Materials & Structures WILEY

Fatigue life assessment of welded joints under sequences of bending and torsion loading blocks of different lengths

Francesco Frendo | **Giuseppe Marulo** | **Andrea Chiocca** | **Leonardo Bertini**

Department of Civil and Industrial Engineering, University of Pisa, Largo Lucio Lazzarino, Pisa, 56122, Italy

Correspondence
F. Frendo, Department of Civil and Industrial Engineering, University of Pisa, Largo Lucio Lazzarino, 56122 Pisa, Italy.
Email: francesco.frendo@unipi.it

Abstract

In this work, the nominal stress concept, the notch stress approach and two critical plane approaches are used to analyse the fatigue endurance of a pipe-to-plate welded joint subjected to complex loading histories. Both the pipe and the plate were made of S355JR steel. Starting from already known fatigue endurance curves obtained for the same specimens under pure bending and pure torsion, a first series of tests was conducted, in which specimens were loaded in bending for a given fraction of the estimated life and then in torsion until failure. A similar series of tests was then carried out by changing the loading order: specimens were firstly loaded in torsion for a given fraction of the estimated endurance and then in bending until failure. The whole test campaign was repeated for two different fractions of the estimated life, that is, 0.3 and 0.45, respectively. After that, additional three series of tests were carried out, in which the specimens were subjected to consecutive sequences of bending and torsion blocks of different lengths (short, medium and long, respectively); the relative length of the bending and torsion block in each series was determined in order to produce the same damage. The experimental results, in terms of total damage at failure, were analysed using the *Palmgren–Miner* hypothesis. For all the assessment methods, the characteristic endurance curves were firstly calibrated on the basis of finite element (FE) analyses and of the experimental results obtained under pure bending and pure torsion loadings. The observed damage at failure resulted always greater than 0.5 for all the employed methods and greater than 1 for most of the tests. The different methods gave similar results, with the critical plane methods giving a slightly more stable damage at failure and a correct determination of the failure location. For all the methods, the damage at failure slightly reduces as the block length shortens.

KEYWORDS

critical plane, loading blocks, multiaxial fatigue, nominal stress, notch stress, welded joints

1 | INTRODUCTION

This paper deals with fatigue life assessment of welded joints under variable amplitude multiaxial loads. Such a complex loading scenario is rarely investigated in the literature due to its high complexity and to the large number of variables involved, even if it appears to be quite frequent in real applications.

 © 2020 Wiley Publishing Ltd.

The nominal stress concept is frequently considered for the fatigue assessment, due to its simplicity, representing the oldest design method originating from times in which a local stress determination [strain gauges or later finite element method (FEM)] was not possible. However, its application requires the calculation of a nominal stress (e.g. based on beam theory), that is possible for simple geometries only, and the allocation of a notch factor or notch case for the selection of the appropriate S–N line, in case of welded joints, fixed by the geometry-dependent FAT class given in design codes.[1,2]

Local approaches, on the other side, are based on local parameters of the stress–strain field, evaluated at the critical locations[3–10] and can provide more reliable fatigue endurance assessments (see, e.g., Bertini et al.[11–12] and Meneghetti[13]), with the main advantages of being independent from the joint geometry. Damage (crack initiation) is, indeed, a local phenomenon that can be tackled by the knowledge of the local stress–strain state and the local material properties as described in Radaj et al.[5]; to this regard, it has also to be observed that the joint stiffness, which is influenced by the plate stiffness and bolt position, may also affect the location of fatigue failure (see, e.g., Bertini et al.[11]).

Among local methods, the notch stress approach (NSA), developed in its modern formulation by Radaj[3] and based on *Neuber*'s concept of microstructural support, is one of the most popular for evaluating the fatigue life of welded joints, being also recommended in guidelines and regulation codes.[2,14] The notches on the component are fictitiously enlarged to a fixed value and, subsequently, the elastic stress range (*von Mises* or maximum principal stress) is estimated at the critical location by finite element analysis.

Alternatively, critical plane approaches rely on the experimental observation that the fatigue cracks on smooth specimens initiate and propagate, in the first stage, in preferred orientations. Indeed, crack nucleation is an extremely local phenomenon, whose scale can be compared with grain size and, at this level, a metallic material cannot be considered as homogeneous and the combination of microstructure and load orientation is believed to result in favourable orientations for crack nucleation. The *Findley* criterion was one of the first critical plane models to be employed. It is a stress-based critical plane approach that maximizes a combination of shear stress amplitude and maximum normal stress occurring over a load cycle in the critical plane. The cyclic shear stress induces the nucleation of cracks, whereas the normal stress influences the crack propagation. The *Findley* criterion has already been applied for fatigue life assessment of welded joints both in its original[15] and also in a modified formulation.[16] The *Fatemi-Socie* is another widely used critical plane approach. It has proved itself as a robust framework for fatigue life assessment, yielding reliable life assessments for a number of structural metals with ductile behaviour and showing shear cracking, including not only several steels and super alloys (Inconel),[10] but also aluminium alloys.[17] On the other side, when failure appears to occur with cracking on maximum tensile plane, such as in case of additively manufactured titanium alloys, this method is not recommended.[18] Also, this method was successfully employed to account for the effects of multiaxial loading conditions, including the effect of variable amplitude loads.[19–23] The fatigue life assessment of welded joints by the *FS* approach, instead, has only been recently proposed.[24,25]

A general review of fatigue criteria for variable amplitude multiaxial loads is given in Carpinteri et al.[26] Considering the cumulative damage, even if different theories have been proposed,[27] the linear damage rule[28] is probably the most widely used one,[29] and the use of *Palmgren–Miner* hypothesis for the fatigue life assessment of welded joints, even under multiaxial loads, is, actually, a common practice.[1,2,30,31] In its original formulation, the *Palmgren–Miner* hypothesis states that failure occurs when the total damage, obtained as the sum of the partial damages produced by each loading cycle of constant amplitude, reaches the unitary value. A first aspect, relevant to welded joints especially in case of multiaxial loading, is that many authors have suggested the use of a total damage D lower than unity.[32,33] Based on results obtained on steel and aluminium welded joints under multiaxial loading conditions, the *IIW* recommend an allowable damage summation equal to $D = 0.5$.[2,34,35] Backstrom and Marquis[36] reviewed a collection of experimental tests under multiaxial loading conditions that are available in the literature and applied a modification of Findley's critical plane approach[32,33] to the 'hot spot' stress finding a better correlation of the experimental data than what was achieved by maximum principal stress. Sonsino[37] and Zhang and Maddox[38] applied the *Palmgren–Miner* hypothesis to a number of variable amplitude loading tests performed on welded joints and found that for the vast majority of the analysed data, the total damage D at failure was less than the theoretical unitary value, with worst case values approaching $D = 0.1$. Then, $D = 0.5$ has to be considered as a conventional engineering estimate, which is a sort of mean value obtained based on the experimentally observed damages.

Aim of the present work is to discuss the capability of the nominal stress concept, the notch stress approach and of some of the most widely employed critical plane approaches in evaluating the fatigue endurance of welded joints under complex loading histories. Before analysing

the experimental results, each assessment method was firstly calibrated based on the results obtained for the same kind of specimen under simple, that is, pure bending and pure torsion, loading conditions, obtaining characteristic endurance curves.

2 | EXPERIMENTAL ACTIVITY

The specimens employed for the experimental campaign consisted of a pipe (external diameter of 64 mm and a thickness of 10 mm) joined by seam welding to a 25-mm thick plate. The weld throat thickness was about 7.1 mm. Both the pipe and the plate were made of structural steel *S355JR* (nominal yield and ultimate strength of $S_y = 355$ MPa and $S_u = 520$ MPa, respectively). The specimen, nearby its end, opposite to the plate, has a circular flange, butt welded to the pipe and used to join the specimen to the loading arm (see Figure 1, left).

Tests were performed thanks to the in-house developed test bench shown in Figure 1 (right) and described in Frendo and Beritini.[39] The bench is composed of two independently controlled hydraulic actuators connected on the opposite sides of a loading arm, which is bolted to the upper part of the specimen. The independent control of each actuator allows to produce on the specimen any desired combination of bending and torsion.

The loading arm has a total length of $2b = 600$ mm. The lower plate of the specimen is fixed to the bench by *M20* bolts. The hydraulic actuators are controlled in order to produce sinusoidal forces with given amplitude, mean load and relative phase shift, that is, $F_1(t) = a_1 \sin(\omega t) + \xi$ and $F_2(t) = a_2 \sin(\omega t + 2\gamma) + \eta$; such forces can be determined in order to obtain the desired bending and twisting moments M_b and M_t in the weld:

$$\begin{aligned} M_b(t) &= [F_1(t) + F_2(t)]h, \\ M_t(t) &= [F_1(t) - F_2(t)]b, \end{aligned} \tag{1}$$

where the bending and torsion arms h and b are related to the pipe and the lever arm lengths, respectively. A prevalent bending load in the welded cross section is obtained imposing $a_1 = a_2$, $\xi = \eta$ and $\gamma = 0$ (in this case also, a shear stress is present; however, its value can be usually neglected, for the given geometry and applied loads). Instead, a torsion load is obtained with $a_1 = a_2$, $\xi = -\eta$ and $\gamma = \pi/2$.

Tests with different blocks of bending and torsion were analysed in this work, for a total of seven test series. Four block load series (i.e. 'B_1', 'B_2', 'T_1', 'T_2') were already published by the authors,[40] whereas three additional series (i.e. '*L*', '*M*' and '*S*') are published here for the first time.

The first two series of tests (named B_1 and B_2 in Table 1) were designed so that the specimens were loaded in bending for two different fractions of the estimated fatigue endurance (i.e. for damages $D_i = 0.3$ and $D_i = 0.45$). Subsequently, they were loaded in torsion until failure.

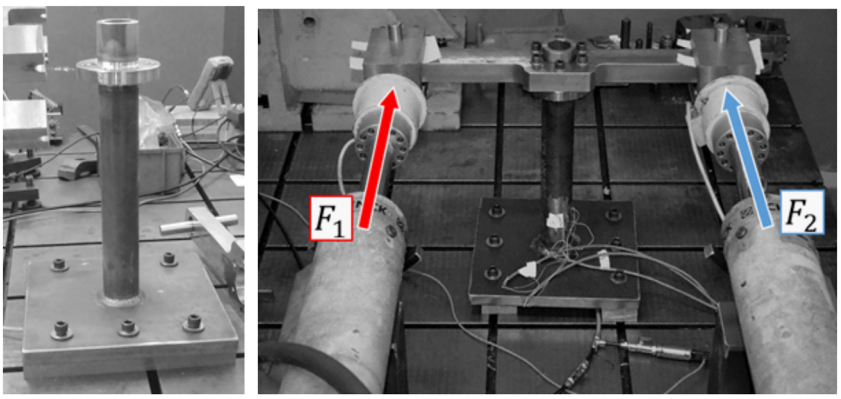


FIGURE 1 Specimen (left) and experimental apparatus (right). The specimen is loaded by two hydraulic actuators attached at the opposite ends of a lever arm; when the actuators act perfectly in phase, the welded joint is subjected to prevalent bending, whereas when they operate opposite in phase, a twisting moment is applied to the joint. In the lower part of the picture the system used to detect the presence of a through-the-thickness crack (based on pressure drop inside the pipe) can also be recognized [Colour figure can be viewed at wileyonlinelibrary.com]

TABLE 1 Test series made of two loading blocks

Test	1st block	D_1	n_1	2nd block	n_2
B_1	Bending	0.30	$2.76 \cdot 10^5$	Torsion	Until failure
B_2	Bending	0.45	$4.14 \cdot 10^5$	Torsion	Until failure
T_1	Torsion	0.30	$3.06 \cdot 10^5$	Bending	Until failure
T_2	Torsion	0.45	$4.59 \cdot 10^5$	Bending	Until failure

Two other series (named 'T_1' and 'T_2' in Table 1) were then obtained inverting the loading sequence: first, the torsion load was applied to reach the desired fraction of the fatigue life (i.e. $D_i = 0.3$ and $D_i = 0.45$); then, the specimens were loaded in bending until failure.

In the last three series (named '*L*', '*M*' and '*S*' in Table 2), fixed length blocks of bending and torsion were applied, consecutively, without interruption until failure. The lengths of bending block were fixed equal to $n_b = 10\,000$, 100 and 10 cycles, for the *L*, *M* and *S* blocks, respectively, whereas the torsion block lengths were calculated in order to obtain the same damage (based on the nominal stress concept), i.e. $D_{ben}/D_{tor} = 1$ if D_{ben} and D_{tor} are the partial damages of the bending and torsion block, for each sequence. The obtained torsion block lengths were equal to $n_t = 11\,000$, 110 and 11 cycles, according to a slightly higher endurable stresses in torsion, as obtained in previous investigations performed on the same kind of specimens[38,41] (see Figure 2).

All the tests were performed with a load ratio $R = 0$.

TABLE 2 Test series composed of many consecutive blocks

Test series	Bending block length	Torsion block length
L	10 000	11 000
M	100	110
S	10	11

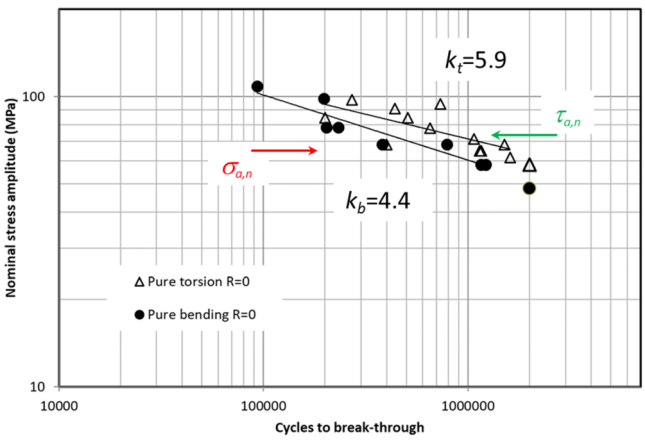


FIGURE 2 Bending and torsion endurance data with $R = 0$ (taken from Bertini et al.[42]); the 50% probability of survival best fit lines are also shown and the inverse slope coefficients given; the amplitude of nominal normal and shear stress used for test are indicated in the graph [Colour figure can be viewed at wileyonlinelibrary.com]

With reference to data shown in Figure 2, the nominal stress ranges in the bending and torsion blocks were selected as described in the following. For the bending blocks, the nominal normal stress amplitude of $\sigma_{a,n} = 64$ MPa ($\Delta\sigma_n = 128$ MPa) was selected, corresponding to an expected fatigue life of $N_b = 9.2{\cdot}10^5$ cycles. Therefore, the fatigue life fractions of $D_i = 0.3$ and $D_i = 0.45$ resulted as bending blocks having lengths of $n_{b,0.3} = 2.76{\cdot}10^5$ and $n_{b,0.45} = 4.14{\cdot}10^5$, respectively.

For the torsion blocks the nominal shear stress amplitude $\tau_{a,n} = 72.5$ MPa ($\Delta\tau_n = 145$ MPa) was selected, in order to have a normal to shear stress ratio equal to $\sigma_n/\tau_n = 0.88$; this allows a comparison of the obtained results with previously published data by the authors.[39,42] For the selected shear stress, the expected endurance is equal to $N_t = 10.2{\cdot}10^5$ cycles (Figure 2), and, therefore, the fatigue life fractions of $D_i = 0.3$ and $D_i = 0.45$ resulted in block lengths of $n_{t,0.3} = 3.06{\cdot}10^5$ and $n_{t,0.45} = 4.59{\cdot}10^5$, respectively.

All the specimens were tested in the as-welded condition. The adopted failure criterion was the presence of a through-the-thickness crack. The occurrence of this kind of damage was easily detected by the sudden drop in the air pressure imposed in the lower chamber of the specimen, before starting each test.

The complete test plan is summarized in Tables 1 and 2. Three tests were repeated for the test series '*B1*', '*B2*', '*T1*' and '*T2*', whereas four tests were repeated for series '*L*', '*M*' and '*S*', for a total of 24 experiments.

3 | EXPERIMENTAL RESULTS

The details of the whole experimental campaign in terms of cycles to failure are given in Table 3. The first column of Table 3 refers to the tests series definitions given in previous Tables 1 and 2, whereas the columns n_b and n_t refer to the number of endured cycles in bending and torsion, respectively; those lengths were necessary to obtain a through-the-thickness fatigue crack. In the last two columns, the total number of cycles and the expected number of cycles to break through, obtained based on the *Palmgren–Miner* hypothesis with $D = 1$ and the nominal stress concept, are given. For all the tests, the nominal stress amplitude were $\sigma_{a,n} = 64$ MPa and $\tau_{a,n} = 72.5$ MPa. The fatigue cracks always originated from the weld root, with very few exceptions, which can be attributed to the intrinsic variability of welds.

For the case of *B* and *T* tests (i.e. in case of two loading blocks), 2 10^6 cycles for the second load block were considered as run-out, whereas for L, M and S tests, a total of 2 10^6 cycles were assumed as run-outs, instead.

TABLE 3 Test results in terms of cycles to break through

Test	$\sigma_{a,n}$ (MPa)	$n_b/10^5$	$\tau_{a,n}$ (MPa)	$n_t/10^5$	$N_{tot}/10^5$	$N_{expected}/10^5$
B_1	64	2.76	72.5	17.9	20.7	9.9
B_1	64	2.76	72.5	12.3	15.1	9.9
B_1	64	2.76	72.5	19.4	22.2	9.9
B_2	64	4.14	72.5	16.6	20.6	9.75
B_2	64	4.14	72.5	5.5	9.5	9.75
B_2	64	4.14	72.5	11.9	15.9	9.75
T_1	64	11.9	72.5	3.06	15.0	9.5
T_1	64	6.2	72.5	3.06	9.3	9.5
T_1	64	14.5	72.5	3.06	17.6	9.5
T_2	64	interr. at 20.0	72.5	4.59	24.5 (run-out)	9.65
T_2	64	19.2	72.5	4.59	23.7	9.65
T_2	64	8.70	72.5	4.59	13.2	9.65
L	64	5.4	72.5	5.9	11.3	9.66
L	64	9.8	72.5	10.8	20.6 (run-out)	9.66
L	64	6.5	72.5	7.2	13.7	9.66
L	64	8.8	72.5	9.7	18.4	9.66
M	64	7.6	72.5	8.4	15.9	9.66
M	64	5.9	72.5	6.5	12.3	9.66
M	64	6.7	72.5	7.4	14.1	9.66
M	64	4.3	72.5	4.8	9.1	9.66
S	64	5.5	72.5	6.1	11.5	9.66
S	64	7.5	72.5	8.2	15.7	9.66
S	64	3.2	72.5	3.5	6.7	9.66
S	64	2.8	72.5	3.1	5.9	9.66

One run-out was obtained for the case of two loading blocks (T_2 test, 10th row in Table 3), where after the first portion of the test in which the specimen was loaded in torsion, 2 10^6 cycles of bending were applied without observing any through-the-thickness crack. In case of L, M and S tests (many consecutive blocks), one run-out was obtained for one of the L tests (14th row in Table 3), where the total number of cycles exceeded 2 10^6 cycles (the test was actually stopped a little bit later and at 2.06 10^6 cycles).

Figure 3 gives an example of the experimentally recorded time history of the loads exerted by the two hydraulic actuators and the evaluated time histories of nominal normal and shear stresses. The plots show a first block of torsion, followed by a transition (load shifting) from the mean torsion load to the mean bending load and by a bending block. It can be easily recognized, both from the actuators loads and from the stress time history, that both the torsion and bending blocks have load ratio $R = 0$.

4 | ANALYSIS OF RESULTS: FATIGUE LIFE ASSESSMENT

The *Palmgren–Miner* hypothesis, commonly suggested in case of variable amplitude loads, was used for evaluating the total damage:

$$D = \sum \frac{n_i}{N_i}, \tag{2}$$

where n_i and N_i are the applied and the endurable load cycles for the considered load. The endurable cycles N_i were determined according to the different damage parameters, belonging to the different analysed methods; these will be briefly summarized in next sections.

The effect of residual stresses was not considered in the following analysis, assuming that stresses induced by the testing loads were high enough, at least locally, to cancel the initial residual stress state.

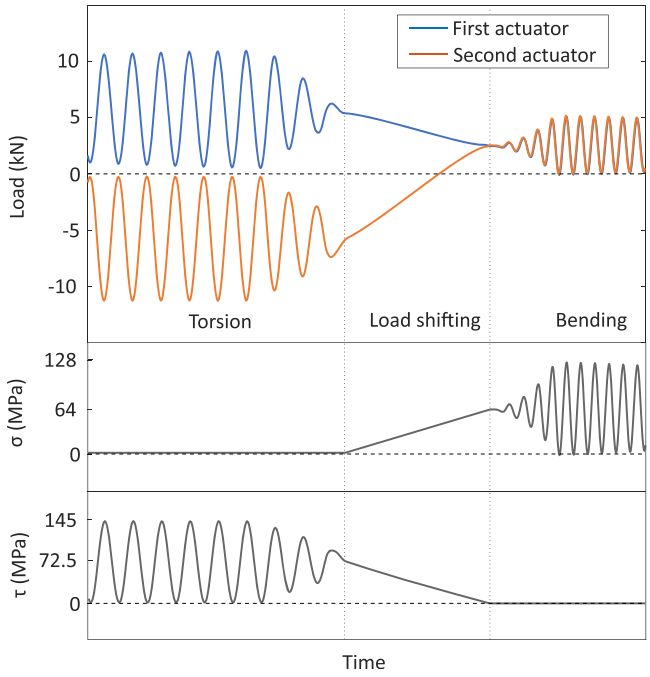


FIGURE 3 Experimental load sequence with highlighted the torsion, bending and load shifting phases (upper plot) and evaluated nominal normal and shear stress (bottom plots) [Colour figure can be viewed at wileyonlinelibrary.com]

4.1 | Fatigue life assessment by the nominal stress concept

When they can be applied, nominal stresses are by far the simpler and straightforward endurable stresses used in fatigue life assessment, and they are usually preferred by engineers working in the industry due to their simplicity. By this method, a detailed knowledge of the local stress–strain is not required and no FE analysis is needed; the analysis is linear elastic, and no plasticity at the weld notches is considered.

The fatigue life is directly related to the nominal values that can be obtained according to common stress formulas, based on beam theory. This method is among those recommended by both the *International Institute of Welding* (IIW)[2] and by the *Eurocode 3*.[1] For the present case, the nominal stress in bending and torsion are easily evaluated by Equations 3 and 4, respectively, where M_b, M_t are the bending and torsion moment, and W_b, W_t are the corresponding strength modulus of the weld section, which can be directly computed for the given weld geometry, described in Section 2:

$$\sigma_n = M_b / W_b, \tag{3}$$

$$\tau_n = M_t / W_t. \tag{4}$$

Besides, the applied nominal stress amplitudes were defined in previous sections and in Table 3. The endurable number of cycles to be used in the *Palmgren–Miner* relationship was determined on the basis of previously determined *S–N* curves (Figure 2).[42] The damage due to bending and torsion were evaluated, separately, by considering different *S–N* curves of nominal normal stress and nominal shear stress.

The damage coming from the mean stress variation (indicated as 'load shifting' in Figure 3) in the load cycle was evaluated considering no variation in the slope coefficient in the high cycle range (i.e. $k' = k$). It is worth noting that the load shifting causes a fatigue cycle having a stress range equal to half the stress range of the main loading cycle and a stress ratio $R = 0$, as the main load cycle (Figure 3).

4.2 | Fatigue life assessment by notch stress approach

Instead of using reference FAT design curves, the experimental data shown in Figure 2 were processed by using the FE model described in Section 4.4 with a linear elastic material behaviour. In addition, for the application of this method, a fictitious radius of $\rho_r = 1\ mm$ was used for all the notches, together with the *von Mises* equivalent stress hypothesis. No mean stress sensitivity factor was used because of the high residual stresses expected in case of welded joints. Two different endurance curves were obtained, one for pure bending and one for pure torsion (Figure 4); inverse slope coefficients of 4.4 and 5.8 were obtained for pure bending and pure torsion, respectively.

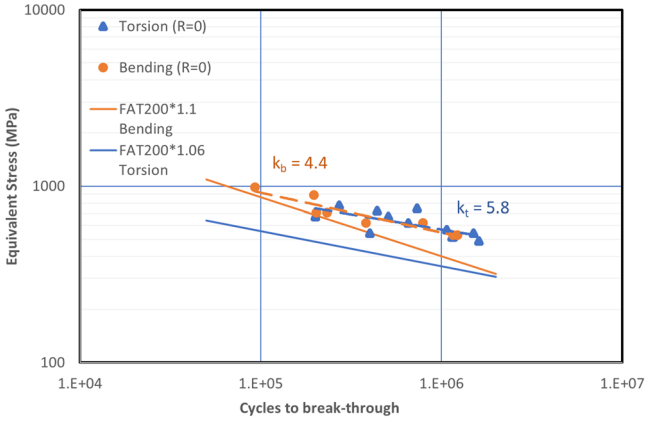


FIGURE 4 von Mises stress versus number of cycles to break through, obtained on the basis of test in pure bending and pure torsion loading, according to the notch stress approach (NSA) [Colour figure can be viewed at wileyonlinelibrary.com]

For the sake of simple comparison, Figure 4 also shows the FAT lines for pure bending and pure torsion taken from Fricke[43]; 1.1 and 1.06 correction factors were used for pure bending and for pure torsion because the FAT values were evaluated for $R = 0.5$.[44] As it can be observed, the FAT line for bending appears in reasonable agreement with experimental data, whereas the FAT line for torsion appears to underestimate the fatigue endurance of the experimental data used in this work. The damage resulting from bending and torsion loading block was then evaluated by Equation 2.

The damage caused by the load shifting from bending to torsion and vice versa was evaluated considering the equivalent stresses due to torsion and that due to bending, separately, as it is recommended in the Eurocode for the nominal stress concept. Also in this case, no variation in the slope coefficient was considered, as for the nominal stress concept, to evaluate the expected number of cycles to failure for half of the applied load.

4.3 | Fatigue life assessment by Fatemi-Socie and Findley critical plane approaches

For the case of *Fatemi-Socie* criterion, the *FS* parameter is given by:

$$FS = \frac{\Delta\gamma}{2}\left(1 + k_{FS}\frac{\sigma_n}{S_y}\right), \tag{5}$$

where it was is assumed $k_{FS} = 0.4$ similarly to what adopted in Hemmesi[24] and the critical plane was assumed as the plane that experiences the maximum value of the *FS* parameter given by Equation 5.

In order to obtain the fatigue curve related to the *FS* parameter, the experimental data already shown in Figure 2 and obtained under pure bending and pure torsion were reinterpreted based on the *FS* parameter given in previous Equation 5. To do this, the FE model described in next section was employed. The *FS* parameter versus number of cycles to break through was so obtained (Figure 5). As it can be observed, data belonging to pure torsion or pure bending appear to belong to a same endurance curve, having inverse slope coefficient equal to 4.1. A similar curve was obtained by the authors in Marulo et al.[45] by using a 1-mm fictitious radius at all the three weld notches. By comparing the present curve (Figure 5) with the one obtained in Frendo and Bertini,[39] it can be observed that, as it can be reasonably expected, the endurance curve depends on the radius used in the FE model.

According to *Findley*,[46] failure occurs on the plane that experiences the maximum value of the parameter:

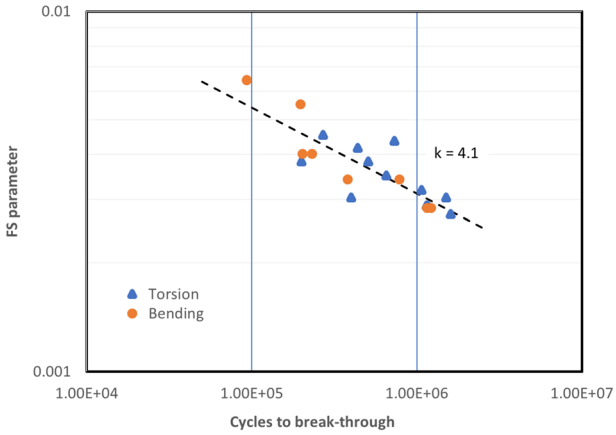


FIGURE 5 FS versus number of cycles to break through, obtained on the basis of test in pure bending and pure torsion loading, according to the Fatemi-Socie parameter [Colour figure can be viewed at wileyonlinelibrary.com]

$$FP = \frac{\Delta\tau}{2} + k_{FP}\sigma_n, \tag{6}$$

where $\Delta\tau$ is the shear range and σ_n is the normal stress acting on the critical plane. It was assumed $k_{FP} = 0.131$, as usually adopted for ductile materials.[47] In the same way as for the *FS* parameter, the experimental data of bending and torsion were reinterpreted based on Equation 6, by the FE analyses described in next Section 4.4. The fatigue endurance curve shown in Figure 6 was so obtained, giving the *Findley's* parameter versus number of cycles to break through. Like the in the previous case, the bending and torsion points belong to the same curve, having an inverse slope coefficient equal to 7.

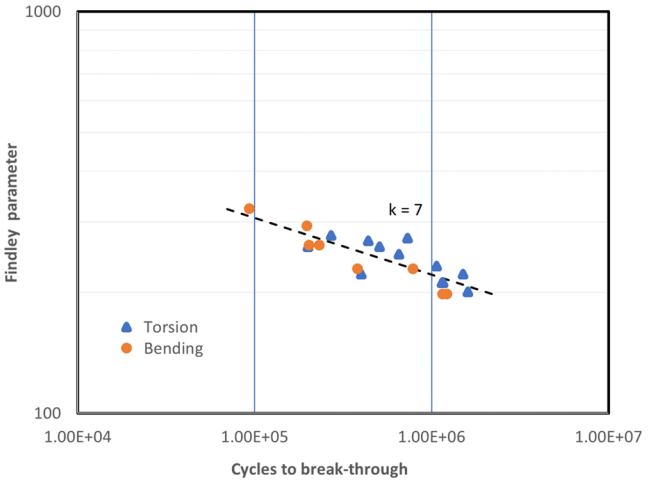


FIGURE 6 FP versus number of cycles to break through, obtained on the basis of test in pure bending and pure torsion loading, according to the Findley parameter [Colour figure can be viewed at wileyonlinelibrary.com]

4.4 | Local damage evaluation by FE analysis

Critical plane methods require a detailed description of the stresses and strains at the critical notches, where the fatigue cracks originate and, in reference to this, the following aspects were considered.

The actual geometry of a seam weld is difficult to be reproduced and varies from specimen to specimen. The fillet seam under investigation presents three sharp notches, that is, two weld toes and a weld root, whose shape are extremely irregular and that can show relevant variations even along the seam in the same specimen. On the basis of pictures taken on the weld cross section, it can be observed that the weld toe on the tube has a significantly larger radius than the radius on the plate side toe or at the weld root (see Figure 7); this is due to the effect of gravity on the molten metal during welding. This causes the weld root and the weld toe on the plate to have a significantly greater notch effect. Based on this experimental observation the FE model was built using the submodelling technique with different radii at the notches as follows (1-mm fictitious radii were used for the *NSA*).

A global model of the specimen with reduced complexity (Figure 8A) is firstly analysed; the small geometrical details that only affect the solution on a local scale were not considered in the global model and a linear elastic material was adopted at this stage. This is based on the observation that the plastic deformations are localized at the stress concentration sites and involve only a small material volume and, therefore, their effect on the global displacements can be neglected. The use of a linear elastic material model allowed to reduce the computational effort and the superposition principle to be used. With this assumption, the global model needed to be evaluated only twice: once for a unitary bending and once for a unitary twisting moment.

The second simulation step is related to the submodel, which involves a portion of the weld seam (Figure 8B). The input for this model is represented by the displacement field computed on its boundary surfaces by means of the global model. For the submodel (Figure 8B), a 2-mm fillet radius was selected on the pipe side weld toe, whereas and a 0.2-mm fillet radius was used on both the plate side weld toe and on the weld root, according to Figure 7; in addition, a nonlinear material model was used in the submodel. For the numerical analyses related to the *NSA*, a linear elastic material and 1-mm fictitious radius notches were used.

An extremely fine mesh was created at the stress concentration sites (Figure 8B). This allows for a detailed

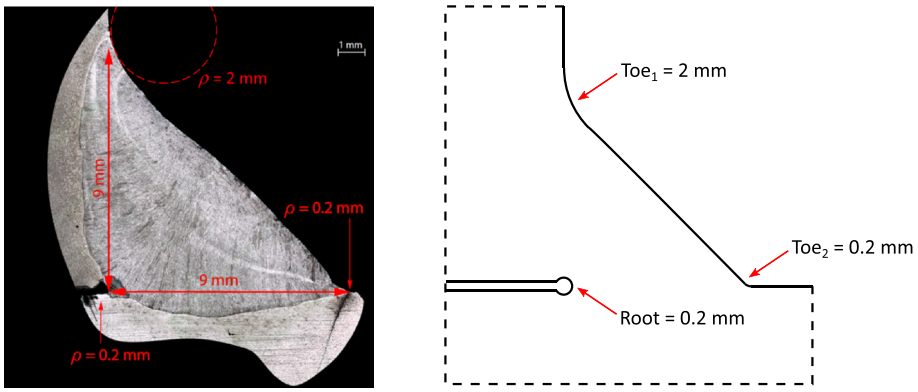


FIGURE 7 Cross section of the seam weld (left) and schematic representation showing the geometrical radii that were assumed at the three notches (right) [Colour figure can be viewed at wileyonlinelibrary.com]

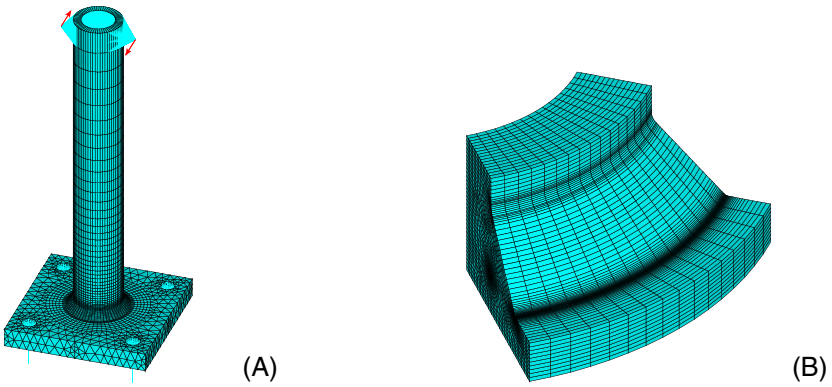


FIGURE 8 View of the global model with torsion loading applied on top (A) and details of the submodel (B) [Colour figure can be viewed at wileyonlinelibrary.com]

description of the stress/strain state in the volume of material where the highest stress/strain gradients are expected. On the notch proximity a mapped mesh made of rectangular hexahedra was generated to obtain a higher level of accuracy, if compared with a free mesh made of tetrahedra with the same number of nodes.[48] The loads in the FE model were applied at top of the specimen, far away from the weld (an example is shown in Figure 8A, for the case of torsion).

The *FS* and the *FP* parameters have to be evaluated considering the variation of the stress and strain tensors between two consecutive load conditions. The loading scheme illustrated in Figure 9 was applied to the FE model, and the results at each load step were stored in separate files, for subsequent analysis. The maximum bending and maximum torsion (Steps 1 and 2) were firstly applied to the FE model, in order to set the initial strain state in the plastic volume. Then, the load sequence from Steps 3 to 9 was used to analyse any load block. A bending cycle is reproduced (Steps 3 to 5) in the FE model, corresponding to max bending to nearly zero and then back to maximum bending. Then, the actuator loads go to mean bending (Step 6) followed by mean torsion (Step 7). Steps 8 to 10 represent a cycle in torsion. Finally, the mean torsion (Step 11) and mean bending (Step 12) are applied.

With reference to critical plane approaches, the damage in each cycle is evaluated considering the stress and strain tensor variations between the load steps as indicated below:

damage due to a bending cycle: Steps 4 to 5;

damage due to a torsion cycle: Steps 9 to 10;

damage due to load shifting from average bending to average torsion: Steps 6 to 7;

damage due to load shifting from average torsion to average bending: Steps 11 to 12.

4.5 | Material model

In the FE analysis, the whole joint was supposed to be constituted of a single and homogeneous material, having the same properties of the base material; it is well known that the material constituting a welded joint does not show homogeneous properties (see, e.g., Marulo et al.[49]) and this was a mere simplification.

The following assumptions were adopted to describe the nonlinear material used in the submodel, in case of the *Findley* and *Fatemi-Socie* critical plane approaches:

- Yield function: *von Mises* equivalent stress.
- Flow rule: *Prandtl–Reuss* flow equation (which is associated with *von Mises* yield function).
- Hardening rule: isotropic hardening, commonly used for stabilized cyclic deformation.[50]

The cyclic stress–strain relationship at yielding was estimated, starting from the static properties of the base material, by the *Ramberg–Osgood* relationship:

$$\varepsilon = \frac{\sigma}{E} + \left(\frac{\sigma}{K'}\right)^{\frac{1}{n'}}. \tag{7}$$

The numerical values of the parameters that appear in the previous equation were obtained based on the empirical relationships suggested for steel components in Lopez and Fatemi[51]; in particular, the cyclic strength coefficient was estimated starting from the ultimate stress (S_u) according to Equation 8

$$K' = 1.16(S_u) + 593, \tag{8}$$

while the cyclic strain hardening exponent can be related to the ultimate (S_u) and the yield (S_y) stresses by Equation 9:

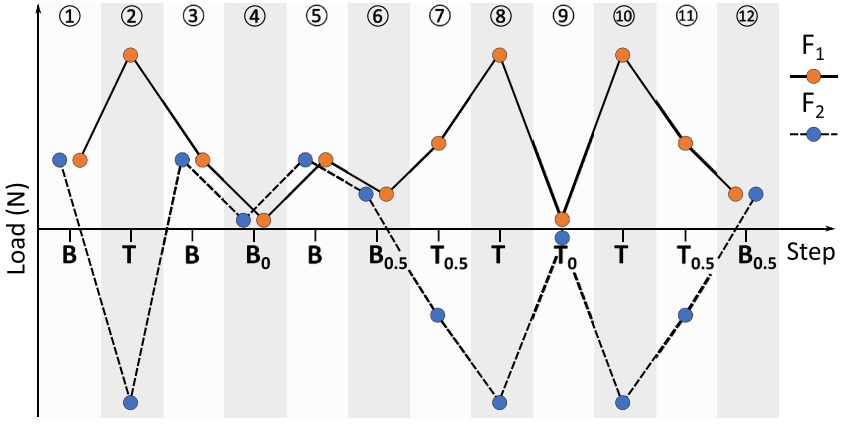


FIGURE 9 Load sequence applied to the FE model (actuator forces definition according to Figure 1) [Colour figure can be viewed at wileyonlinelibrary.com]

$$n' = -0.33\left(\frac{S_y}{S_u}\right) + 0.40. \quad (9)$$

When applied to the S355JR steel under investigation ($S_y = 355$ and $S_u = 520$ MPa), the following parameters were obtained: $K' = 1185$ MPa and $n' = 0.175$.

4.6 | Numerical procedure for critical plane determination

As already stated, the critical plane was assumed as the plane where the variation of the selected parameter in the load cycle assumes its maximum value. For any given location (node in the FE model), this plane was determined starting from the stress and strain tensors variation between two load steps ($\Delta\sigma$ and $\Delta\varepsilon$). This was accomplished by an automatic routine appositely developed, where the stress and strain tensors, (3 × 3) matrices, were rotated according to an x–y–z intrinsic *Euler* angles set, in small increments of 2.5° along all possible directions. Generally speaking, two rotations would be sufficient to determine a plane orientation, the third rotation not introducing any variation in the plane orientation; however, this would require summing up the two components of the shear strain range in each plane to check when the maximum of the parameter is obtained. With the developed routine, instead, the maximum value of the parameter is directly obtained by considering all possible orientation of the reference frame.

The above illustrated procedure was repeated for all the nodes along the main notches, where failure could take place, to identify the critical locations and the critical plane orientations under the different loading conditions.

5 | RESULTS AND DISCUSSION

5.1 | Nominal stress concept

Figure 10 on the left shows the damages at failure obtained by the nominal stress method, whereas Figure 10 on the right shows the same results in the form of occurred versus expected number of cycles to break through (see Table 3 for numerical data); data are aligned at almost the same expected life, since tests were planned in this way, based on the nominal stress concept (i.e. data given in Figure 2).

As it can be observed in the left plot, a different damage at failure was observed for each block sequences. The average values range from 1.78 for the two blocks sequence to 1.03 for the 'short' block sequence and looks like the average damage for each test series tends toward unity, as the length of the block shortens. In addition, for the analysed tests, the damage at failure was greater than 1 in most of the tests, always greater than the conventional 0.5 value suggested by *IIW* and lower than 1 only in few cases.

Considering all the results, with the exceptions of run-outs, the overall average damage and the standard deviation resulted 1.49 and 0.49, respectively.

It is also worth noting that the damage resulting from load shifting is negligible, even if the elementary *Palmgren–Miner* modification of the *S–N* curve (i.e. no variation in the slope of the S–N curve) is used. Indeed, the stress amplitude is half the nominal stress amplitude used for the tests and $\sigma_{a,n} = 32$ MPa and $\tau_{a,n} = 36.25$ MPa, respectively. The expected endurance with these stress amplitudes (with no variation in the slope coefficient) is about 3 10^7 and 8 10^7 cycles for bending and torsion loading, respectively (see Figure 2); when these endurances are used in the *Palmgren–Miner* relationship (Equation 2), no appreciable damage turns out.

5.2 | Notch stress approach

Very similar results were obtained with the application of the *NSA*; the damage of each test is reported in Figure 11 on the left, while occurred versus expected number of cycles to break through are shown in Figure 11 on the right. Also, in this case, the damage is higher than 1 for almost all the tests, with an average value, computed over

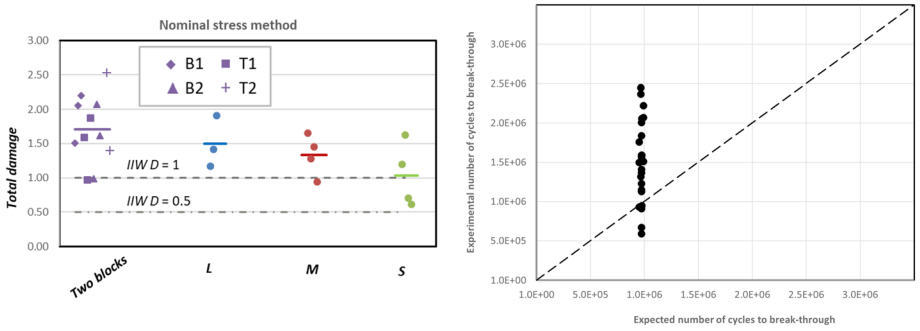


FIGURE 10 Total damage at break through for each load block according to Palmgren–Miner hypothesis, based on the nominal stress concept (left); for the two block histories, the four test series are distinguished; experimental versus expected number of cycles based on the nominal stress concept and according to the Palmgren–Miner hypothesis (right) [Colour figure can be viewed at wileyonlinelibrary.com]

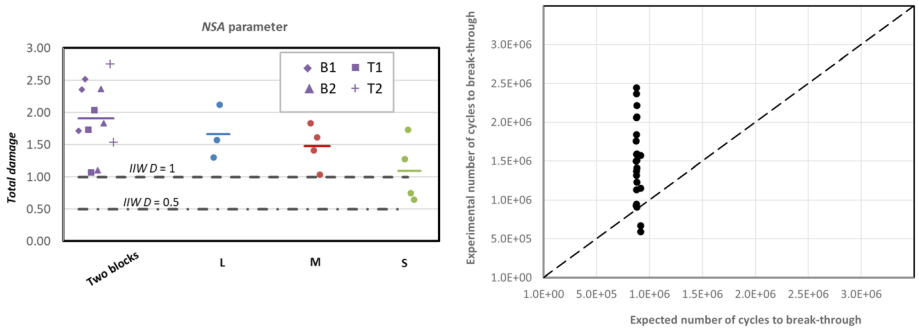


FIGURE 11 Total damage at break through evaluated according to Palmgren–Miner hypothesis by using the NSA approach (left) (for the two block histories, the four test series are distinguished); experimental versus expected number of cycles based on the NSA method and according to the Palmgren–Miner hypothesis (right) [Colour figure can be viewed at wileyonlinelibrary.com]

TABLE 4 Maximum von Mises equivalent stress in the weld root and weld toes for both bending and torsion loading, according to the NSA (root, Toe_1 and Toe_2 are indicated in Figure 7)

Position	Bending (MPa)	Torsion (MPa)
Root	343	454
Toe_1	579	575
Toe_2	209	211

all the test, of 1.65 and a standard deviation of 0.56. By considering a fictitious radius of 1 mm in all the notches, the weld toe on the pipe side (Weld Toe_1 in Figure 7) was obtained as the critical location for failure initiation, as indicated in Table 4. This was not confirmed by test outcomes and suggests that the actual geometry of the joint has to be described in the analysis to correctly obtain the failure location, in the present case.

As for the nominal stress concept, also in this case, the damage coming from the load shift appeared not to be significant, resulting always lower than 1% of the total damage.

5.3 | Fatemi-Socie and Findley parameters

The *FS* and *FP* parameters evaluated for each loading cycle by the FE model previously described are given in the second column of Table 5. The node number is also shown in Figure 12, showing an enlarged view of the central portion of the notch at the weld root. The last column in Table 5 gives the number of cycles to break through, based on the adopted critical plane parameter, that is, on the plot shown in Figures 5 and 6, respectively; this data is useful to evaluate the damages shown in Figures 13 and 14 according to the *Palmgren–Miner* hypothesis (Equation 2).

As it will be discussed with reference to Figures 13 and 14, similar results were obtained by the *FS* and *FP* parameters. The node where the adopted parameters is at maximum is practically the same; a very subtle difference can be observed only in the case of 'bending to torsion', as shown in Table 5 and Figure 12.

The nodes of the FE model that experience the highest critical plane parameter in the different loading conditions are located at the weld root, in agreement with the observed failures and are very close among each other, so that it can be considered that the failure location is always in the middle of the root notch (see Figure 12).

It has to be considered that the critical plane for each loading cycle has a different orientation. Nevertheless, in order to simplify the analysis and considering the small process volume where the fatigue crack nucleates, it was assumed as a reasonable approximation to sum up the damages as they occurred on the same node and always

TABLE 5 FS and Findley parameter, corresponding node number in the FE model and number of cycles to break through, for the different loading block

Loading cycle	Critical plane parameter	Node number	N_{FS}
Fatemi-Socie			
Bending	$3.0\ 10^{-3}$	3134	$1.10\ 10^{6}$
Torsion	$2.97\ 10^{-3}$	2556	$1.24\ 10^{6}$
Bending to torsion	$1.98\ 10^{-3}$	2542	$6.70\ 10^{6}$
Torsion to bending	$2.05\ 10^{-3}$	2542	$6.50\ 10^{6}$
Findley			
Bending	209 MPa	3134	$1.50\ 10^{6}$
Torsion	223 MPa	2556	$9.50\ 10^{5}$
Bending to torsion	146.6 MPa	3134	$2.10\ 10^{7}$
Torsion to bending	151.5 MPa	2542	$1.60\ 10^{7}$

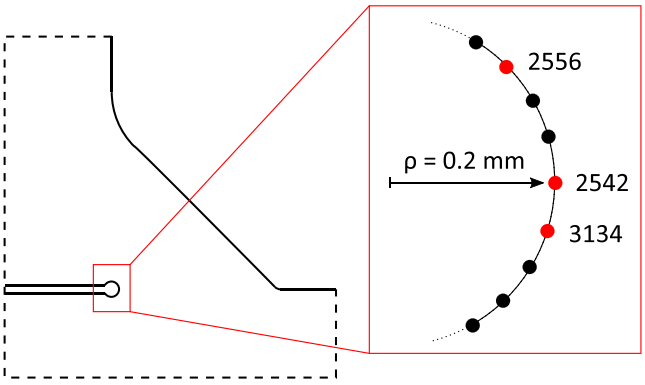


FIGURE 12 Enlarged view of the nodes at the weld root; nodes in red are those where the highest values of the FS and FP parameters were obtained for the four loading cycles [Colour figure can be viewed at wileyonlinelibrary.com]

on the same plane. This is a mere simplification and a more accurate procedure can be developed in future works.

By using the *FS* and *FP* parameters obtained by the FE analyses (given in Table 5), the damages shown in Figures 13 and 14 on the left were obtained. The same results are given in the plots on the right side of the figures, in terms of occurred versus expected number of cycles to break through. Also in this case, the damage at break through is always greater than 0.5. The FS parameter provided a slightly smaller dispersion. Considering all the tests with the exceptions of run-outs, the average damage at failure resulted about 1.22 and 1.26 for the *FS* and *FP* parameters, whereas the standard deviation resulted 0.41 and 0.47, respectively.

By comparing results given in the left plots of Figures 10 to 14, it can be observed that a slightly more stable damage at break through was obtained with the critical plane approaches.

The relatively larger dispersion in the expected number of cycles to break through obtained for critical plane approaches, if compared with the right plot in Figure 10, is simply related to the fact that all the test series were planned for the same expected endurance on the basis of the nominal stress concept (i.e. data in Figure 2) and testifies the difference of the methods used for the fatigue endurance assessment (i.e. nonlinear analysis and detailed geometry in case of *FS* and *FP* parameters).

It is worth noting that the damage associated to load shifting is very low also in case of critical plane approaches, even if this contribution obtained according to *FS* parameter is significantly higher than that obtained with all the other methods. In particular, with reference to 'S' blocks, which experiences many load variations from bending to torsion and vice versa, the damage associated to load shifting goes from about 2% of total damage at failure (average value) if *FS* parameter is used, to 0.6% with *FP* parameter and 0.3% with the *NSA*.

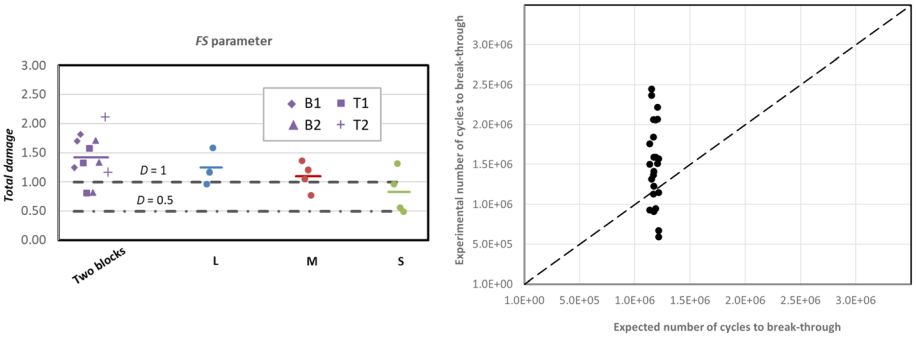


FIGURE 13 Total damage at break through evaluated according to Palmgren–Miner hypothesis by using the FS parameter (left) (for the two block histories, the four test series are distinguished); experimental versus expected number of cycles based on the FS parameter and according to the Palmgren–Miner hypothesis (right) [Colour figure can be viewed at wileyonlinelibrary.com]

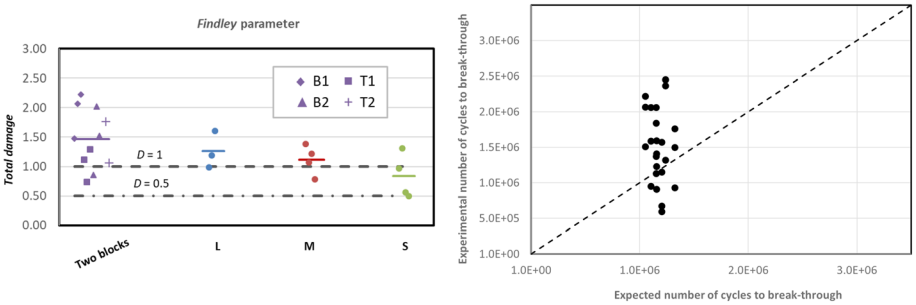


FIGURE 14 Total damage at break through evaluated according to Palmgren–Miner hypothesis by using the Findley parameter (left) (for the two block histories, the four test series are distinguished); experimental versus expected number of cycles based on the Findley parameter and according to the Palmgren–Miner hypothesis (right) [Colour figure can be viewed at wileyonlinelibrary.com]

6 | CONCLUSIONS

From the research activity and based on the obtained results the following main conclusion can be drawn:

- When it can be applied, the nominal stress method is by far the simplest method in terms of analysis and computation time; for the relatively simple geometry that was investigated, the results obtained by the nominal stress approach, if compared with the results obtained by the more complex methods (requiring at least a linear FE analysis), can be considered fairly good.
- For the present study, the application of the *NSA*, gave results in very close agreement with the nominal stress concept; this was mainly due to the fact the endurance curves were calibrated on the same available data base and to the fact the both the nominal stress approach and the NSA are based on a linear elastic analysis.
- Critical plane approaches, at the cost of a greater effort necessary for model development and data analysis gave similar results to the other methods, with a slightly lower variability of the damage observed at failure for the different loading sequence.
- An accurate description of the actual weld geometry is mandatory to be able to correctly determine the fatigue crack initiation site; this was accomplished only by the critical plane approaches, in the present case.
- For all the employed methods the damage at failure appeared to depend on the loading history and, in particular, on the block length; the damage at failure reduced as the length of the loading blocks shortened; the observed damage at failure was greater than one in most of the experiments.
- The fatigue assessment of welded joints under complex loads remains an open subject and a unified approach is not available, yet.

7 | NOMENCLATURE

a_1, a_2	amplitudes of the actuators load history
b	twisting moment arm
D	damage
D_1	expected damage related to the first loading block
D_{ben}	damage in the bending block cycles
D_{tor}	damage in the torsion block cycle
E	Young's modulus
F_1, F_2	Forces exerted by the hydraulic actuators
FP	damage parameter according to the *Findley* critical plane hypothesis
FS	damage parameter according to the *Fatemi-Socie* critical plane hypothesis
h	bending moment arm
k_{FS}	coefficient used in the *FS* parameter
k_{FP}	coefficient used in the *FP* parameter
K'	cyclic strength coefficient in the *Ramberg–Osgood* relationship
n_1, n_2	number of cycles in the first and second loading block
n'	cyclic strain hardening exponent in the *Ramberg–Osgood* relationship
$n_{b,0.3}$	number of cycles in the bending block, related to an expected damage of 0.3
$n_{b,0.45}$	number of cycles in the bending block, related to an expected damage of 0.45
n_i	number of applied cycles
$n_{t,0.3}$	number of cycles in the torsion block, related to an expected damage of 0.3
$n_{t,0.45}$	number of cycles in the torsion block, related to an expected damage of 0.45
N_i	expected endurable loading cycles for the given applied loading
N_b	number of cycles of the bending block
N_t	number of cycles of the torsion block
N_{tot}	total number of cycles for any given loading block
M_b	bending moment
M_t	t moment
R	load ratio
S_u	ultimate stress
S_y	yield stress
W_b	strength modulus under bending loading
W_t	strength modulus under torsion loading
γ	phase shift between the actuators load
$\Delta\gamma$	shear strain range in the *FS* parameter
$\Delta\bar{\sigma}$	nominal normal stress range related to load shifting cycle
$\Delta\bar{\tau}$	nominal shear stress range related to load shifting cycle
$\Delta\sigma_n$	nominal normal stress range
$\Delta\tau_n$	nominal shear stress range
ε	uniaxial strain in the *Ramberg–Osgood* relationship
ξ, η	mean load exerted by the hydraulic actuators
σ	uniaxial stress in the *Ramberg–Osgood* relationship
σ_n	nominal normal stress
$\sigma_{a,n}$	nominal normal stress amplitude of the fatigue cycle
$\sigma_{n,max}$	normal stress acting on the critical plane
$\tau_{a,n}$	nominal shear stress
$\tau_{a,n}$	

nominal shear stress amplitude of the fatigue cycle

ω angular frequency in the actuators load

ORCID

Francesco Frendo https://orcid.org/0000-0002-7472-4664

Andrea Chiocca https://orcid.org/0000-0002-1472-4398

REFERENCES

1. EN. ,"Eurocode3: design of steel structures. Fatigue," 1993.
2. Hobbacher A. *Recommendations for Fatigue Design of Welded Joints and Components*. Cham: Springer International Publishing; 2016.
3. Radaj D. *Design and Analysis of Fatigue Resistant Welded Structures*. Abington, Cambridge: Woodhead Publishing; 1990.
4. Radaj D, Lazzarin P, Berto F. Generalised Neuber concept of fictitious notch rounding. *Int J Fatigue*. 2013;51:105-115.
5. Radaj D, Sonsino CM, Fricke W. *Fatigue Assessment of Welded Joints by Local Approaches*. Abington, Cambridge, England: Woodhead publishing Limited; 2006.
6. Sonsino C, Fricke W, De Bruyne F, Hoppe A, Ahmadi A, Zhang G. Notch stress concepts for the fatigue assessment of welded joints—background and applications. *Int J Fatigue*. 2012;34(1):2-16.
7. Lazzarin P, Tovo R. A notch intensity factor approach to the stress analysis of welds. *Fatigue Fract Eng Mater Struct*. 1998;21 (9):1089-1103.
8. Tovo R, Lazzarin P. Relationships between local and structural stress in the evaluation of the weld toe stress distribution. *Int J Fatigue*. 1999;21(10):1063-1078.
9. Meneghetti G, Lazzarin P. Significance of the elastic peak stress evaluated by FE analyses at the point of singularity of sharp v-notched components. *Fatigue Fract Eng Mater Struct*. 2007;30 (2):95-106.
10. Fatemi A, Socie D. A critical plane approach to multiaxial fatigue damage including out-of-phase loading. *Fatigue Fract Eng Mater Struct*. 1988;11(3):149-165.
11. Bertini L, Frendo F, Marulo G. Effects of plate stiffness on the fatigue resistance and failure location of pipe-to-plate welded joints under bending. *Int J Fatigue*. 2016;90:78-86.
12. Bertini L, Frendo F, Marulo G. Fatigue life assessment of welded joints by two local stress approaches: the notch stress approach and the peak stress method. *Int J Fatigue*. 2018;110: 246-253.
13. Meneghetti G, Campagnolo A, Avalle M, et al. Rapid evaluation of notch stress intensity factors using the peak stress method: comparison of commercial finite element codes for a range of mesh patterns. *Fatigue Fract Eng Mater Struct*. 2017;41 (5):1044-1063.
14. Fricke W. Guideline for the fatigue assessment by notch stress analysis for welded structures. *Int Instit Welding*. 2010;13:2240-2208. 43, 44,65, 106
15. Bolchoun A, Sonsino C, Kaufmann H, Melz T. Multiaxial random fatigue of magnesium laser beam-welded joints—experimental results and numerical fatigue life evaluation. *Procedia Eng*. 2015;101:61-68.
16. Bäckström M. Multiaxial fatigue life assessment of welds based on nominal and hot spot stresses. Ph.D. thesis. Laapeenranta University, Finland; 2003.
17. Gates N, Fatemi A. Notched fatigue behavior and stress analysis under multiaxial states of stress. *Int J Fatigue*. 2014;67:2-14.
18. Fatemi A, Molaei R, Sharifimehr S, Phan N, Shamsaei N. Multiaxial fatigue behavior of wrought and additive manufactured ti-6al-4v including surface finish effect. *Int J Fatigue*. 2017;100 (Part 1):347-366.
19. Gladskyi M, Fatemi A. Notched fatigue behavior including load sequence effects under axial and torsional loadings. *Int J Fatigue*. 2013;55:43-53.
20. Gates NR, Fatemi A. Multiaxial variable amplitude fatigue life analysis using the critical plane approach, part I: un-notched specimen experiments and life estimations. *Int J Fatigue*. 2017; 105:283-295.
21. Gates NR, Fatemi A. Multiaxial variable amplitude fatigue life analysis using the critical plane approach, part II: notched specimen experiments and life estimations. *Int J Fatigue*. 2018; 106:56-69.
22. Gates NR, Fatemi A. Experimental fatigue crack growth behavior and predictions under multiaxial variable amplitude service loading histories. *Eng Fract Mech*. 2017;174:80-103.
23. Stephens RI, Fatemi A, Stephens RR, Fuchs HO. *Metal Fatigue in Engineering*. 2nd edition ed. John Wiley & Sons; 2001.
24. Hemmesi K, Farajian M, Fatemi A. Application of the critical plane approach to the torsional fatigue assessment of welds considering the effect of residual stresses. *Int J Fatigue*. 2017; 101:271-281.
25. Chen X, An K, Kim K. Low-cycle fatigue of 1cr-18ni-9ti stainless steel and related weld metal under axial, torsional and 90 out-of-phase loading. *Fatigue Fract Eng Mater Struct*. 2004; 27(6):439-448.
26. Carpinteri A, Spagnoli A, Vantadori S. A review of multiaxial fatigue criteria for random variable amplitude loads. *Fatigue Fract Eng Mater Struct*. 2017;40(7):1007-1036.
27. Fatemi A, Yang L. Cumulative fatigue damage and life prediction theories: a survey of the state of the art for homogeneous materials. *Int J Fatigue*. 1998;20(1):9-34.
28. Miner MA. Cumulative damage in fatigue. *J Appl Mech*. 1945; 12(3):159-164.
29. Gurney TR. *Cumulative Damage of Welded Joints*. Cambridge England: Woodhead Publishing; 2006.
30. Backstrom M, Marquis G. Interaction equations for multiaxial fatigue assessment of welded structures. *Fatigue Fract Eng Mater Struct*. 2004;27(11):991-1003.
31. Sonsino C. Multiaxial fatigue assessment of welded joints-recommendations for design codes. *Int J Fatigue*. 2009;31(1): 173-187.
32. Witt M and Zenner H, "Multiaxial fatigue behavior of welded flange-tube connections under combined loading. Experiments and lifetime prediction," ICBMFF5, 1997.
33. Sonsino C, Kueppers M. Multiaxial fatigue of welded joints under constant and variable amplitude loadings. *Fatigue Fract Eng Mater Struct*. 2001;24(5):309-327.
34. Sonsino C and Wiebesiek J, "Assessment of multiaxial spectrum loading of welded steel and aluminium joints by modified equivalent stress and Gough-Pollard algorithms," IIW Doc. No. XIII-2158r1–07/XV-1250r1–07, 2007.

35. Wiebesiek J, Sonsino C. New results in multiaxial fatigue of welded aluminium joints. *IIW Doc*. 2010;13:2314-2310.
36. Backstrom M, Marquis G. A review of multiaxial fatigue of weldments: experimental results, design code and critical plane approaches. *Fatigue Fract Eng Mater Struct*. 2001;24(5):279-291.
37. Sonsino C. Fatigue testing under variable amplitude loading. *Int J Fatigue*. 2007;29(6):1080-1089.
38. Zhang Y-H, Maddox S. Investigation of fatigue damage to welded joints under variable amplitude loading spectra. *Int J Fatigue*. 2009;31(1):138-152.
39. Frendo F, Bertini L. Fatigue resistance of pipe-to-plate welded joint under in-phase and out-of-phase combined bending and torsion. *Int J Fatigue*. 2015;79:46-53.
40. Bertini L, Frendo F, Marulo G. Fatigue endurance of welded joints subjected to different blocks of bending and torsion loading. In: *Procedia Struct Integrity*. Vol.2 Elsevier; 2016:3531-3538.
41. Marquis G, Backstrom M, and Siljander A, "Multiaxial fatigue damage parameters for welded joints: design code and critical plane approaches," in Proc. First North European Engineering and Science Conference, 1997.
42. Bertini L, Cera A, Frendo F. Experimental investigation of the fatigue resistance of pipe-to-plate welded connections under bending, torsion and mixed mode loading. *Int J Fatigue*. 2014;68:178-185.
43. Fricke W. *IIW Recommendations for the Fatigue Assessment of Welded Structures by 32 Notch Stress Analysis*. International Institute of Welding: Woodhead Publishing; 2012.
44. Sonsino CM. A consideration of allowable equivalent stresses for fatigue design of welded joints according to the notch stress concept with rref = 1.00 mm and 0.05 mm. Weld World 2009;53:R64–R75.
45. Marulo G, Frendo F, Bertini L, Fatemi A. On the application of a critical plane approach to the life assessment of welded joints. *Procedia Eng*. 2018;213:448-458.
46. Findley WN, A theory for the effect of mean stress on fatigue of metals under combined torsion and axial load or bending. No. 6, Engineering Materials Research Laboratory, Division of Engineering, Brown University, 1958.
47. Margetin M, Durka R, Chmelko V. Multiaxial fatigue criterion based on parameters from torsion and axial S-N curve. *Frattura Ed Integrità Strutturale*. 2016;10(37):146-152. https://doi.org/10.3221/IGF-ESIS.37.20
48. Baumgartner J, Bruder T. An efficient meshing approach for the calculation of notch stresses. *Welding in the World*. 2013;57(1):137-145.
49. Marulo G, Baumgartner J, Frendo F. Fatigue strength assessment of laser welded thin-walled joints made of mild and high strength steel. *Int J Fatigue*. 2017;96:142-151.
50. Socie D, Marquis G. *Multiaxial Fatigue*. Society of Automotive Engineers, Inc.; 2007.
51. Lopez Z, Fatemi A. A method of predicting cyclic stress–strain curve from tensile properties for steels. *Mater Sci Eng A*. 2012;556:540-550.

How to cite this article: Frendo F, Marulo G, Chiocca A, Bertini L. Fatigue life assessment of welded joints under sequences of bending and torsion loading blocks of different lengths. *Fatigue Fract Eng Mater Struct*. 2020;43:1290–1304. https://doi.org/10.1111/ffe.13223